ORIGINAL ARTICLE

TUBB4A mutations result in specific neuronal and oligodendrocytic defects that closely match clinically distinct phenotypes

Julian Curiel[1,†], Guillermo Rodríguez Bey[2,†], Asako Takanohashi[3,4], Marianna Bugiani[5], Xiaoqin Fu[1], Nicole I. Wolf[5], Bruce Nmezi[2], Raphael Schiffmann[6], Mona Bugaighis[1], Tyler Pierson[7], Guy Helman[3,8,9], Cas Simons[8], Marjo S. van der Knaap[5], Judy Liu[1,‡], Quasar Padiath[2,‡] and Adeline Vanderver[3,4,9,10,*,‡]

[1]Center for Neuroscience Research, Children's National Health System, Children's Research Institute, Washington, DC 20010, USA, [2]Department of Human Genetics, University of Pittsburgh, Pittsburgh, PA 15260, USA, [3]Center for Genetic Medicine Research, Children's National Health System, Children's Research Institute, Washington, DC 20010, USA, [4]Division of Neurology, Children's Hospital of Philadelphia, Philadelphia, PA 19104, USA, [5]VU University Medical Center, Amsterdam, The Netherlands, [6]Institute of Metabolic Disease, Baylor Scott & White Research Institute, Dallas, TX 75204, USA, [7]Departments of Pediatrics and Neurology, Cedar Sinai Medical Center, Board of Governors Regenerative Medicine Institute, Los Angeles, CA 90048, USA, [8]Institute for Molecular Bioscience, University of Queensland, Brisbane, Australia, [9]Department of Neurology, Children's National Health System, Washington, DC 20010, USA and [10]Perlman School of Medicine, University of Pennsylvania, Philadelphia, PA 19104, USA

*To whom correspondence should be addressed at: Children's Hospital of Philadelphia, 3615 Civic Center Blvd., Abramson Research Center 516H, PA 19104, USA. Tel: 215-590-1719; Fax: 215-590-1771; Email: vandervera@email.chop.edu

Abstract

Hypomyelinating leukodystrophies are heritable disorders defined by lack of development of brain myelin, but the cellular mechanisms of hypomyelination are often poorly understood. Mutations in *TUBB4A*, encoding the tubulin isoform tubulin beta class IVA (Tubb4a), result in the symptom complex of hypomyelination with atrophy of basal ganglia and cerebellum (H-ABC). Additionally, *TUBB4A* mutations are known to result in a broad phenotypic spectrum, ranging from primary dystonia (DYT4), isolated hypomyelination with spastic quadriplegia, and an infantile onset encephalopathy, suggesting multiple cell types may be involved. We present a study of the cellular effects of *TUBB4A* mutations responsible for H-ABC (p.Asp249Asn), DYT4 (p.Arg2Gly), a severe combined phenotype with hypomyelination and encephalopathy (p.Asn414Lys), as well as milder phenotypes causing isolated hypomyelination (p.Val255Ile and p.Arg282Pro). We used a combination of histopathological, biochemical and cellular approaches to determine how these different mutations may have variable cellular effects in neurons and/or oligodendrocytes. Our results demonstrate that specific mutations lead to either purely

neuronal, combined neuronal and oligodendrocytic or purely oligodendrocytic defects that closely match their respective clinical phenotypes. Thus, the DYT4 mutation that leads to phenotypes attributable to neuronal dysfunction results in altered neuronal morphology, but with unchanged tubulin quantity and polymerization, with normal oligodendrocyte morphology and myelin gene expression. Conversely, mutations associated with isolated hypomyelination (p.Val255Ile and p.Arg282Pro) and the severe combined phenotype (p.Asn414Lys) resulted in normal neuronal morphology but were associated with altered oligodendrocyte morphology, myelin gene expression, and microtubule dysfunction. The H-ABC mutation (p.Asp249Asn) that exhibits a combined neuronal and myelin phenotype had overlapping cellular defects involving both neuronal and oligodendrocyte cell types *in vitro*. Only mutations causing hypomyelination phenotypes showed altered microtubule dynamics and acted through a dominant toxic gain of function mechanism. The DYT4 mutation had no impact on microtubule dynamics suggesting a distinct mechanism of action. In summary, the different clinical phenotypes associated with *TUBB4A* reflect the selective and specific cellular effects of the causative mutations. Cellular specificity of disease pathogenesis is relevant to developing targeted treatments for this disabling condition.

Introduction

Hypomyelinating leukodystrophies (HLs) are heritable disorders of the development and maintenance of brain myelin. They were initially identified and diagnosed based on magnetic resonance (MRI) features of T2 hyperintensity with only mildly abnormal or normal T1 signal (1,2). The molecular causes of HLs are varied, but have been thought to relate primarily to glial dysfunction. This dysfunction can include abnormalities in myelin proteins (*PLP1* in Pelizaeus Merzbacher disease –OMIM #312080), protein translation (*POLR3A, POLR3B, POLR1C* in 4H syndrome- OMIM #607694, 614381, 616494) and gap junction proteins linking astrocytes and oligodendrocytes (*GJC2* in Pelizaeus Merzbacher-like disease- OMIM #608804). Interestingly, the recent identification of heterozygous mutations of *TUBB4A* (encoding the Tubulin Beta Class IVA isoform: Tubb4a) in individuals with hypomyelination indicates that other CNS cell types besides oligodendrocytes may be involved in HLs. To date, more than 30 heterozygous pathogenic mutations have been identified in *TUBB4A* that can result in a broad phenotypic spectrum including primary dystonia (DYT4-OMIM#128101) (3,4), spastic diplegia (5–7) infantile encephalopathy (1,8), isolated hypomyelination, (9) and Hypomyelination with Atrophy of Basal ganglia and Cerebellum (H-ABC-OMIM #612438)) (1,3,4,6–23). Of note, other tubulin related disorders have predominantly neuronal manifestations (24), suggesting our existing understanding of the cellular involvement in hypomyelinating leukodystrophies likely underestimates the complexity of oligodendrocyte-neuronal interactions.

This heterogeneity suggests that different *TUBB4A* mutations may have variable cellular effects that can predominantly affect either neurons, oligodendrocytes or both types of cells. We report the cellular effects of different heterozygous *TUBB4A* mutations, including the common mutation responsible for H-ABC (c.745 G > A; p. p.Asp249Asn), (1,10) DYT4 (c.5 G > A; p.Arg2Gly) (3), and three additional mutations, including two previously published variants associated with isolated hypomyelination and milder phenotypes of spastic paraplegia (c.763 G > A; p.Val255Ile and c.845 G > C, p.Arg282Pro) (9) and a very recently published mutation (c.1242 C > G; p.Asn414Lys) associated with severe encephalopathy and early death (25).Using a combination of histo-pathological, biochemical and cell biology approaches, we demonstrate that the different *TUBB4A* mutations result in cell-specific effects that closely match the clinical phenotypes associated with them. The correlation between the phenotypes and the selective cellular effects of each mutation may also represent how phenotypic heterogeneity may be generated in other neurodegenerative conditions.
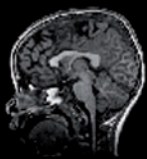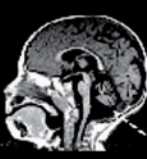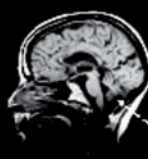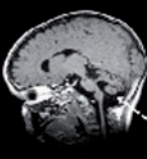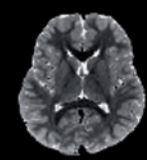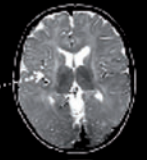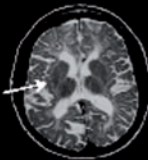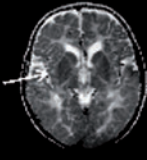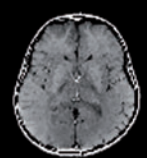
Materials and Methods

Selection of mutations and clinical description of individuals

For these experiments, we chose to analyze five different *TUBB4A* mutations representing different associated phenotypes (Table 1, Fig. 1). All mutations were causative for the disease phenotype in the heterozygous state. Clinical data were collected under an IRB approved protocol at the Children's National Health System and the VUMC in Amsterdam. MRIs and clinical data were reviewed by M.S.v.d.K. and A.V. In addition, existing literature was reviewed for clinical features and molecular characterization of published individuals (*n* = 107) to better describe the phenotypic spectrum of this disorder, (1,3,4,6–10,12–23) and how mutations studied here correspond to known phenotypes associated with heterozygous *TUBB4A* mutations. DYT4 individuals (p.Arg2Gly variant) present with an adult presentation of whispering dysphonia and abnormal gait, but without involvement of myelination, cerebellum or abnormalities of the basal ganglia on neuroimaging. Classic H-ABC individuals with the canonical p.Asp249Asn mutation present with a milder course including relatively preserved motor and cognitive skills typically presenting after a year of age. H-ABC is characterized by hypomyelination combined with atrophy of the putamen, caudate nucleus and cerebellum on both neuroimaging and pathologic data. Two variants associated with isolated hypomyelination on MRI 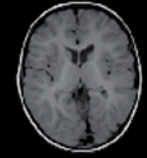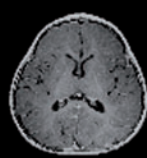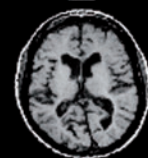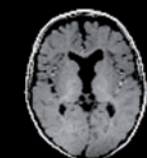and milder later onset phenotypes, p.Val255Ile and p.Arg282Pro (9), were selected in view of the lack of apparent structural involvement of the basal ganglia, with variable cerebellar involvement. A mutation in an individual evaluated by M.S.v.d.K. and N.I.W. (p.Asn414Lys) (25) with a severe infantile onset presentation was selected in view of lack of myelination, cerebellar atrophy and preserved basal ganglia on neuroimaging, but clinically severe encephalopathy and early death.

Pathologic characterization of variants p.Asp249Asn and p.Asn414Lys

Brain samples from three individuals with mutations in *TUBB4A*, two with the common p.Asp249Asn and one with p.Asn414Lys, were collected and analyzed at the VU University Medical Center, Amsterdam. After embedding in paraffin, the tissue was sectioned at 6 μm and stained with hematoxylin and eosin (H&E) according to standard methods. Additionally, tissue sections were incubated with antibodies against the following epitopes: glial fibrillary acidic protein (GFAP; Millipore, 1: 1000),

| Disease description	Whispering Dysphonia (DYT4)	H-ABC	Isolated Hypomyelination	Isolated Hypomyelination	Early infantile encephalopathy
Amino acid change	p.Arg2Gly	p.Asp249Asn	p.Val255Ile	p.Arg282Pro	p.Asn414Lys
Nucleic acid change	c.4C>G	c.745G>A	c.763G>A	c.845G>C	c.1242C>G
Sagittal T1					
Axial T2					
Axial T1	5 yo healthy male	4 yo female	5 yo female	45 yo female	3 yo male
Imaging features	No structural Abnormalities	Hypomyelination and atrophy of the basal ganglia, cerebellum, and corpus callosum	Hypomyelination and atrophy of cerebellum	Hypomyelination and atrophy of the cerebellum	Severe hypomyelination, normal basal ganglia, severe atrophy of cerebellum
Clinical features	Dysphonia, gait affected, and dystonia	Ataxia, dystonia and intellectual disability	Spastic quadriparesis, ataxia	Spastic paraparesis, intellectual disability	Severe intellectual disability, motor deterioration, epilepsy, early death
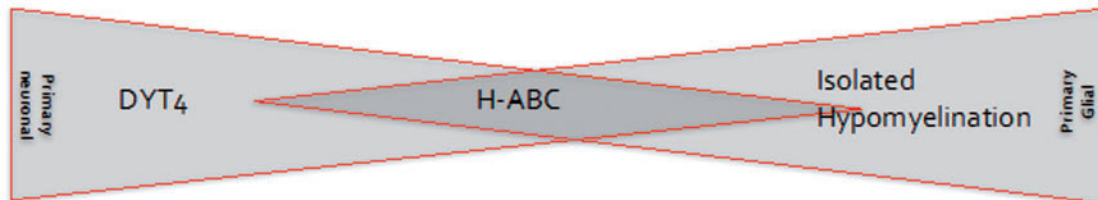
Figure 1. MRI features in individuals with *TUBB4A* mutations. Sagittal T1 (top), Axial T2 (middle) and Axial T1 images (bottom) images are shown. Individuals are shown corresponding to the mutations tested in cellular models. The R2G mutation associated with DYT4 and whispering dysphonia/dystonia is not shown as there are no gross structural abnormalities associated with it. Individual 1 was a normal 12-year-old female to illustrate normal MRI findings. Individual 2 was a 13-year-old male with classic H-ABC and D249N mutation. Individual 3 (V255I) was a 5-year-old female with isolated hypomyelination on neuroimaging and clinical features of spastic quadriparesis and ataxia. Individual 4 (R282P) is a 45-year-old female with isolated hypomyelination on neuroimaging and clinical features of spastic quadreplegia. Individual 5 (N414K) is a 3-year-old male with severe early onset encephalopathy, severe intellectual disability, motor deterioration, epilepsy, and early death. Note the absence of a putamen in individual 2 with preserved putamen in individuals 3, 4 and 5 (thin arrow). Note cerebellar atrophy present in all affected cases (dotted arrow) as well as abnormal T2 signal in the white matter. The schematic below represents the relative contribution of oligodendrocyte versus neuronal mechanisms of disease to the phenotype. MRIs for D249N, V255I, and R282P modified from Pizzino *et al.* (2014).

proteolipid protein (PLP; AbDSerotec, 1: 3000), neurofilaments (SMI31 and SMI311; Covance, 1: 1000) and human leukocyte antigen (HLA)-DR (DAKO; 1: 400). Sections were deparaffinized and rehydrated. Endogenous peroxidase activity was quenched by incubating the slides in 0.3% hydrogen peroxide in methanol. Heat-induced antigen retrieval was performed in citric acid (0.01 M, pH6) using microwave irradiation for 15 min on low setting. Tissue sections were incubated overnight with primary antibodies, and the staining was developed with 3, 3'-diaminobenzidine as chromogen. Sections were counterstained with hematoxylin, dehydrated and mounted with polyvinyl alcohol medium with DABCO (Sigma). Negative controls by omitting the primary antibody were included in each experiment and were essentially blank (not shown).

Construction of wild type and mutated eGFP-TUBB4A expression vectors

The *TUBB4A* ORF was PCR amplified from a human *TUBB4A* cDNA containing plasmid (Accession No: NM_006087, OriGene

Table 1. Characteristics of published individuals with *TUBB4A* mutations

Number of previously published mutations, including those within this manuscript, excluding 19 individuals with DYT4 presentations from two affected families	Excluding DYT4 presentations, n = 88
	Number of canonical H-ABC affected individuals with p.D249N mutation, n = 35 (40% of non DYT4 presentations)
	The remainder of mutations were private mutations occurring in two or fewer families with the exception of c.730G>A (occurring in four apparently unrelated individuals) and c.785G>A (occurring in three unrelated individuals).
Gender	37 females and 51 males
Median age of first symptoms	6.5 months (range 1–60)
Median age of last follow up	11 years (range 2–55)
Number achieving independent ambulation	33/77 (43%); only 13 with preserved ambulation over time; individuals who never achieved independent ambulation were significantly younger at presentation (4 months, SD 7.1) than individuals who achieved ambulation (18 months, SD 13.9) and achieving ambulation was significantly associated with D249N (Fisher exact, $P = 0.02$).
Number achieving speech/verbal communication	46/78 (59%); individuals who never achieved speech were significantly younger at presentation (3.5 months, SD 3.2) than individuals who achieved speech (18 months, SD 13.6) and achieving speech was significantly associated with D249N (Fisher exact, $P=0.0001$)
Presence of seizures	Individuals who had seizures were significantly younger at presentation (4 months, SD 12.1) than individuals who achieved ambulation (12 months, SD 12.0) and absence of seizures significantly associated with D249N (Fisher exact, $P=0.02$).
Presence of cognitive impairment	17 were described as cognitively normal (24%), 33 with mild cognitive impairments (46%) and 21 with severe cognitive impairments (30%)
Presence of dystonia during clinical course	70/85 (82%) had impairments related to dystonia

Technologies, Inc.). The PCR product was then cloned into the pEGFP-C1 vector (Clontech). Point mutations were introduced into pEGFP-TUBB4A using the QuikChange II Site-Directed Mutagenesis Kit (Agilent Technologies) as per manufacturer's instructions. All plasmids were sequenced to ensure the specificity of site-directed mutagenesis. Mutation nomenclature is relative to the transcription start site of TUBB4A.

Tubulin protein stability assay

HEK293 cells (cultured in DMEM medium using standard conditions) were transfected with the various GFP-tagged tubulin constructs using Lipofectamine LTX (Invitrogen). Twenty-four hours after transfection, cells were treated with 200 ng/μl of cyclohexamide for 12 h and protein lysates were collected from the transfected cells. Immunoblotting was carried out using chicken anti-GFP (Abcam, ab13970), mouse anti-Tubb4 (Abcam, ab11315) and mouse anti-GAPDH (Thermo, MA515738). Membranes were incubated with IRDye 800CW (green channel) and IRDye 680LT (red channel) secondary antibodies (Licor). Blots were then imaged using the Odyssey CLx Imaging System (Licor) and band intensities quantified.

Microtubule polymerization assay

Microtubule polymerization assays were performed as previously described (26). TUBB4A-GFP-transfected HEK cells were harvested in BRB80 buffer and lysates were cleared by ultracentrifugation at 15, 000 RPM at 4 °C for 20 min. 1 mM GTP and purified bovine brain tubulin (0.1 mg/ml) (Cytoskeleton) were added to the supernatant along with graded addition of taxol at 1 μM, 10 μM and finally 100 μM taxol in DMSO for 1 h at 37 °C. Samples were then centrifuged for 45 min at 37 °C at 100, 000 g. Supernatant pellet fractions were analyzed by Western blot

analysis using antibodies for rat-α-tubulin (TUBA, Abcam) and mouse-GFP (Invitrogen) and imaged using the Licor system.

EB3 polymerization assay in HeLa cells

HeLa cells were seeded at a density of 1×10^6 cells per well and co-transfected with 2.5 μg of the total plasmid DNA of TUBB4A-GFP and EB3-Cherry using Lipofectamine 3000 (Invitrogen). Images were acquired on an inverted epifluorescence microscope (IX-81, Olympus America Inc., Melville, NY, USA) equipped with high numerical aperture lenses (Apo 603 NA 1.45, Olympus) and a stage top incubator (Tokaihit, Japan) maintained at 37 °C at a rate of two captures per second for 90 total images. Fluorescence excitation was carried out using solid-state lasers (Melles Griot, Carlsbad, CA) emitting at 488 nm (for green) and 561 nm (for red) fluorophores. Images were acquired with a 12-bit cooled CCD ORCA-ER (Hamamatsu Photonics) with a resolution of 1280×1024 pixels (pixel size = 6.45 mm^2). The camera, lasers, and shutters were all controlled using Slidebook 6 (Intelligent Imaging Innovations, Denver, CO). Analysis of time lapse was performed on ImageJ software to calculate EB3 comet velocity. Assays were performed twice with experimental duplicates.

Cerebellar granule transfection

Cerebellar granule neurons were isolated from C57/B6 mice at post-natal day 4 (27), and plated at a density of 1×10^6/well. Neurons were then transfected at DIV 3 with Lipofectamine 2000 (Invitrogen) and TUBB4A-GFP plasmids. 48 h later, neurons were fixed and stained with anti-mouse Tuj1 (Santa Cruz) and anti-rabbit Map2 (Covance) antibodies and appropriate secondary antibodies. Microscopy was carried out using confocal imaging (Olympus) and analyzed using ImageJ and Metamorph Premiere software.

Oli-neu cell culture, transfection and morphological analysis

Oli-neu cells (a gift from Dr. Patrizia Casaccia) were maintained in DMEM/F12 (GIBCO) with 2% B27 (GIBCO). For differentiation, B27 was reduced to 0.5% and medium was supplemented with T3 (30 ng/ml; Sigma). Cells were transfected with 5 μg of total plasmid DNA using either the AMAXA system, program A-033 (Lonza) or Lipofectamine LTX (Invitrogen), as per manufacturer's instructions. Immunocytochemistry was carried out using transfected Oli-neu cells grown on poly-D-lysine (Sigma) treated coverslips using chicken anti-GFP (Abcam, ab13970) and mouse anti-CNPase (Millipore, NE1020) primary antibodies and Cy3-conjugated anti-chicken and FITC-conjugated anti-mouse secondary antibodies (Jackson Immuoresearch). Coverslips were mounted using antifade Mounting medium with DAPI (Vectashield), and imaged using a Leica CTR5000 fluorescence microscope using identical exposure settings. The investigator was blinded to the identities of the different transfected constructs while carrying out morphological analysis.

Quantitative real-time reverse transcription PCR (qRT-PCR)

Total RNA was extracted from transfected Oli-neu cells using TRIzol (Ambion). After treatment with DNAase (Invitrogen) 1 μg of RNA was used for cDNA synthesis with qScript™ cDNA SuperMix (Quanta). QT-PCR was performed on an ABI 7900HT real-time thermocycler (Life Technologies) and analyzed using the ΔΔCT method (28) and normalized to β-actin as the internal control. PCR primers used are listed in Supplementary Material.

Results

Phenotypic characterization of mutations and affected individuals

The mutations undergoing functional characterization (Fig. 1) were selected for their representation of different clinical and radiologic phenotypes. These phenotypes (Fig. 1) are consistent with groups of individuals emerging from an analysis of 107 published cases (Table 1).

Pathologic characterization of variants p.Asp249Asn and p.Asn414Lys

To evaluate the consequences of the p.Asp249Asn and p.Asn414Lys mutations, we carried out a histo-pathological examination and comparison of brain tissue from these patients. Macroscopic examination of the brain from the two individuals with classical H-ABC associated with the p.Asp249Asn mutation in *TUBB4A*, showed atrophy of the cerebellum, particularly the vermis, and to a lesser extent the basis of the pons and pyramids in the brainstem. The surface of the cerebral hemispheres was unremarkable (data not shown). Coronal sections of the cerebral hemispheres revealed a very thin, slightly yellowish putamen and a small caudate nucleus, while the thalamus and globus pallidus were normal. The lateral ventricles were mildly enlarged and the white matter appeared grayish. Examination of the brain sample from an individual with the p.Asn414Lys mutation, showed a similar degree of cerebellar atrophy, also affecting the vermis; while coronal sections of the putamen and caudate nucleus had a normal appearance. The lateral ventricles were moderately enlarged and the corpus callosum was

thin. The white matter of the deep and subcortical areas, the internal capsule, anterior commissure and corpus callosum was grayish and virtually undistinguishable from the gray matter (data not shown).

On microscopic examination, the cerebellar cortex of the two individuals with classical H-ABC was atrophic with a severely paucicellular granular layer (Fig. 2A). The molecular layer was narrowed and slightly gliotic. There was only a minor dropout of Purkinje cells, but the remaining Purkinje cells showed markedly swollen dendrites and axons (Fig. 2B). A similar cerebellar cortical pathology was also seen in the individual with the severe combined phenotype associated with the p.Asn414Lys mutation (Fig. 2C and D), although the thinning of the granular layer was somewhat less severe. In all three individuals, the cerebellar white matter was pale, especially in the cerebellar cortical folia.

The cerebral cortex was normal in all three subjects. The degeneration of the putamen was subtotal in both classical H-ABC individuals (Fig. 2E) with few, if any remaining neurons and astrogliosis (Fig. 2F). The caudate nucleus also showed slight neuronal loss and mild astrogliosis. In the individual with the severe combined phenotype, the putamen and caudate nucleus were unremarkable (Fig. 2G and H). The thalamus and globus pallidus were intact in all three individuals.

At high magnification, microscopy revealed a severe loss of oligodendrocytes in the white matter of both classical H-ABC individuals together with sparse axonal spheroids (Fig. 2I and J). By contrast, the density of white matter oligodendrocytes was increased with the p.Asn414Lys mutation, and no axonal swellings or spheroids were found (Fig. 2K and L). The lack of myelin appeared to be related to both hypomyelination and mild myelin degeneration, as a few macrophages could be focally found in perivascular regions. The axons were much better preserved. In the white matter of all individuals, immunohistochemistry demonstrated strong activation of microglia (Fig. 2M and O) and moderate isomorphic reactive astrogliosis, more prominent around blood vessels (Fig. 2N and P). There was a marked lack of myelin in the cerebral white matter of the deeper and subcortical cerebral areas of the two patient samples when compared with the control (Fig. 2Q and S), which was more severe with the p.Asn414Lys mutation. The U-fibers were also involved. These results are consistent with a recently published report independently describing the pathology associated with the p.Asn414Lys mutation (25).

TUBB4A mutations do not impact protein stability, but differentially affect microtubule dynamics

The selected mutations are located in several different functional domains of TUBB4A (Fig. 3A). The p.Arg2Gly mutation is located in a highly conserved Met-Arg-Glu-Ile (MREI) region that is present in all beta-tubulin isotypes. It is known to interact with the Asn249 amino acid site and plays a role in microtubule stability (Fig. 3A) (10,29). A mutation at this site could theoretically alter the relative abundance of Tubb4a protein. The p.Val255Ile mutation is located near the GTP binding domain of Tubb4a protein, which is involved in binding alpha and beta tubulin (Fig. 3A). The nearby p.Arg282Pro mutation occurs on the M-loop of the Tubb4a, which forms lateral interactions between tubulin subunits to help stabilize the tubulin polymer (Fig. 3A). Based on their respective locations, both are expected to affect tubulin polymerization. The p.Asp249Asn mutation affects an integral amino acid that interacts with residue Arg2, thought to play a role in the stability of assembled microtubules. Finally,
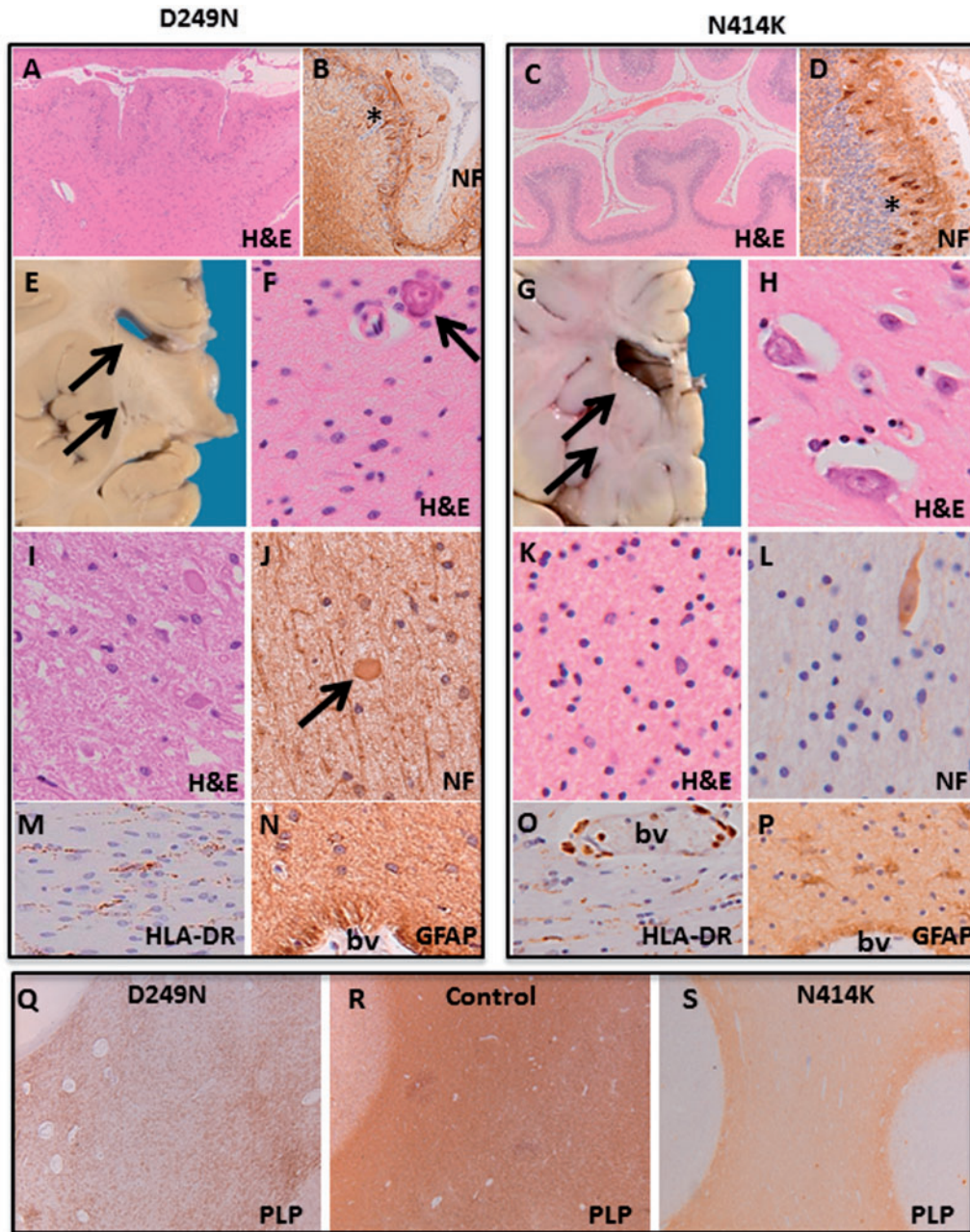
Figure 2. Neuropathology of TUBB4A-related diseases. Images in the top left box are D249N mutation pathology figures and images in the top right box are N414K mutation pathology figures. (**A**) In classical H-ABC (D249N mutation), the cerebellar cortex is severely atrophic with massive loss of granular neurons; stain against neurofilaments (NF) (**B**) shows swelling of Purkinje cell dendrites and axons (asterix). (**C**) In early onset encephalopathy (N414K mutation), the cerebellum also shows severe cortical atrophy with enlargement of the sulci and thinning of the granular layer; stain against NF (**D**) shows swellings of Purkinje cell axons and dendrites (asterix). (**E**) On macroscopic examination of a classical H-ABC brain, the putamen and, to a lesser degree, the caudate nucleus is not recognizable (arrows) on this coronal brain slice cut at the level of the anterior hippocampus. (**F**) This corresponds microscopically with loss of striatal neurons. Note also the small perivascular calcification (arrow). (**G**) In the individual with the severe combined phenotype, the putamen and caudate nucleus are preserved (arrows), and (**H**) there is no loss of striatal neurons. (**I–L**) Microscopic examination of the cerebral white matter reveals lack of oligodendrocytes (dark round nuclei) (I) and presence of axonal swelling and spheroids (I, J; arrow in J) in classical H-ABC, whereas the number of oligodendrocytes is increased in the severe combined phenotype (K) and no spheroids are present (L). Note the white matter neuron normally expressing NF. (**M–P**) In both H-ABC (M,N) and the severe combined phenotype (R,S), the white matter also shows strong activation of rod-shaped microglia (O,P) with accruing of some plump macrophages in the perivascular spaces (bv) (P) and moderate isomorphic reactive astrogliosis with scattered hypertrophic cells in the parenchyma and around blood vessels (N,P). The bottom box has immunohistochemical stain against the major myelin protein proteolipid protein (PLP) from D249N (**Q**), control (**R**), and N414K (**S**) brain slices. (R) PLP staining in frontal lobe of normal brain. (Q,S) Images show severe lack of myelin in the frontal lobe in classical H-ABC (Q) and an even more profound lack in the severe combined phenotype (S).
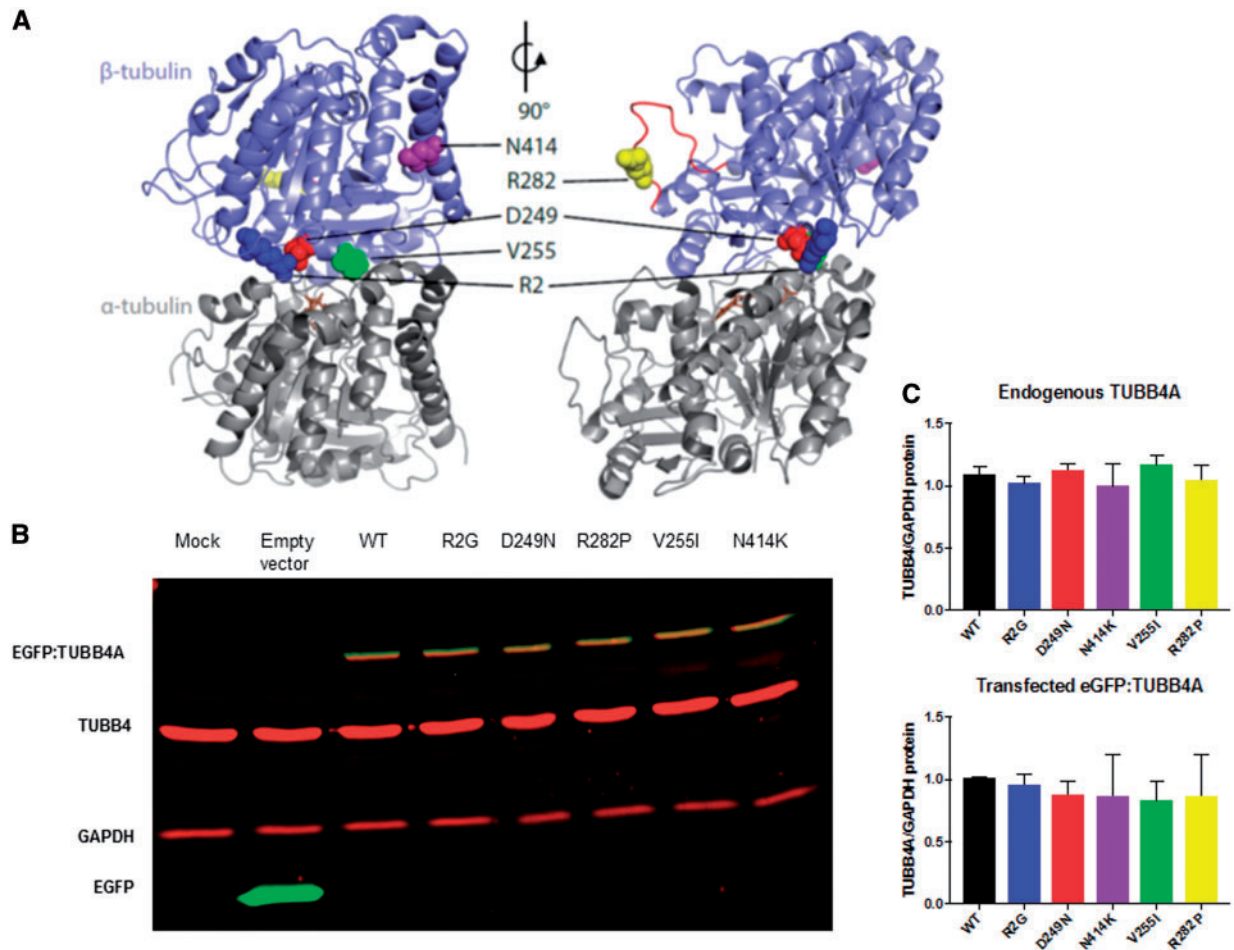
Figure 3. 3D Mapping of TUBB4A mutations and their impact on protein stability. (**A**) Schematic of αβ-tubulin heterodimer structure. TUBB4A (sky blue) is shown bound to alpha tubulin (gray) with the GTP (brown) binding site and the M-loop (red). [JC1] The amino acids R2 (dark blue), D249 (red), V255 (green), R282 (yellow), and N414 (purple) are shown as spheres. The structural model of human TUBB4A (UniProt accession P04350) was generated by ProMod3 v1.0.2 through the SWISS-MODEL web service (47) using the PDB structure 1JFF as a template (29). Pymol (Schrödinger, LLC.) was used to generate the images. (**B**) Representative immunoblot of protein lysates from HEK293 cells transfected with wild type and mutant tubulin for protein stability assays. Immunoblots were simultaneously probed with anti TUBB4 (red), anti GAPDH (red) as a loading control and anti-GFP (green) antibodies. The transfected TUBB4A migrates higher than endogenous TUBB4 due to the presence of the GFP tag and appears as a yellow band due to co-staining of both anti TUBB4 and anti GFP antibodies. (**C**) Quantitation of endogenous and GFP tagged TUBB4A levels relative to GAPDH show no significant alterations between different mutations. ($n = 3$ independent experiments for each construct).

the mutation p.Asn414Lys sits in the beta tubulin H12 helix that is the docking site for kinesins and other motor proteins and is thought to alter their activity (30), but have also been shown to alter polymerization dynamics at the plus- and minus-ends of microtubules (31).

Protein stability assays indicated that none of these mutations affected the steady-state levels of TUBB4A protein (Fig. 3B). HEK293 cells transfected with mutant EGFP-TUBB4A constructs had similar levels of endogenous or exogenous TUBB4 levels compared with wild-type (WT) transfections (Fig. 3C).

We then analyzed how TUBB4A-GFP bearing pathogenic mutations might affect the overall tubulin polymerization (Fig. 4A). We used ultracentrifugation to separate microtubules from unincorporated free tubulin. Free tubulin remained in the supernatant (S) and tubulin polymers were in the pellet (P) (Fig. 4B). Mutations p.Arg2Gly (DYT4), p.Asp249Asn (H-ABC) and the severe phenotype p.Asn414Lys, did not affect WT tubulin incorporation into microtubules when compared with WT TUBB4A (Fig. 4B); however, mutations p.Val255Ile and p.Arg282Pro, result in a decreased incorporation of the WT tubulin into

microtubules as more of the native TUBA remained in the supernatant while the entirety of the TUBB4A-GFP was present in the polymerized form (P). (Fig. 4B). This was not a result of differences between the incorporation of WT and mutant tubulin-GFP (Fig. 4C). These results suggest that the p.Val255Ile and p.Arg282Pro might act through a dominant toxic gain of function mechanism.

To further study the dynamics by assessing the rate of tubulin polymerization, we performed live imaging of the plus-end microtubule binding protein, EB3. We co-transfected HELA cells with EB3-cherry and the TUBB4A-GFP plasmids, and used EB3-cherry to track the growing end of microtubules. The velocities of WT (1.67 μm/s), and p.Arg2Gly (1.61 μm/s), were indistinguishable from one another, indicating the same rate of tubulin polymerization (Fig. 4D). Interestingly, p.Asp249Asn (1.85 μm/s), and p.Asn414Lys (1.87 μm/s) both caused statistically increased rates of polymerization over controls while the two mutants p.Val255Ile (1.47 μm/s) and p.Arg282Pro (1.31 μm/s) mutants had diminished velocity of the EB3 comets, indicating a slower rate of polymerization, which is consistent with the decreased
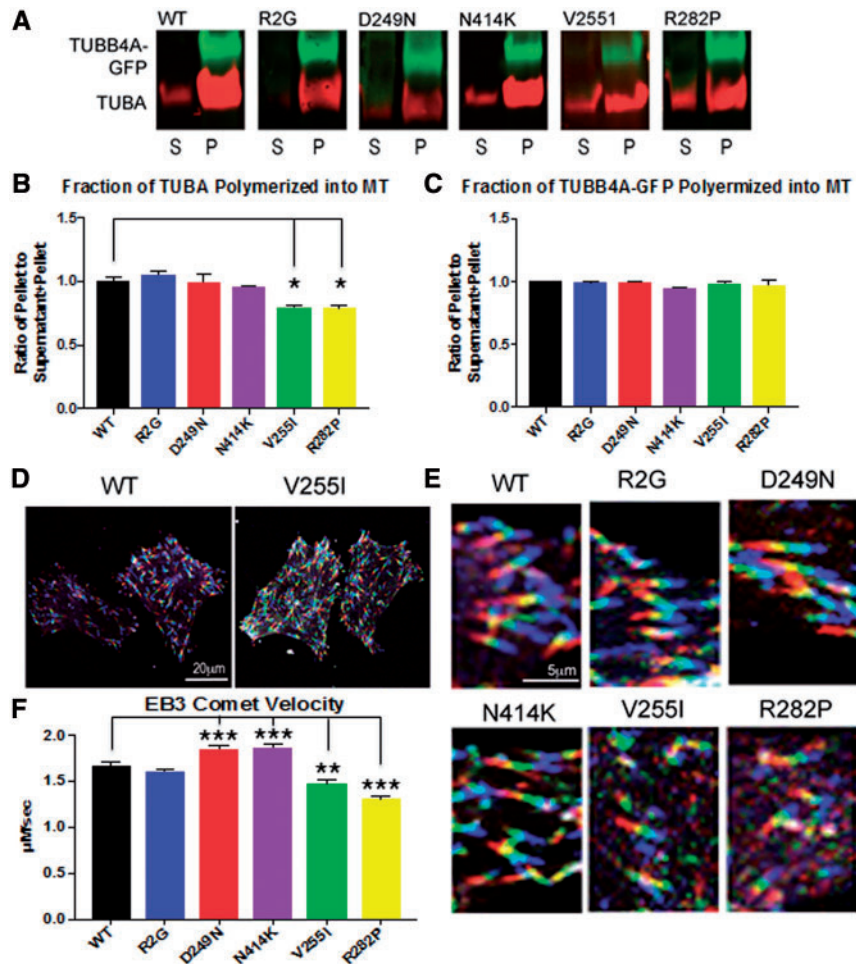
Figure 4. TUBB4A mutations cause abnormal tubulin polymerization (**A**) The microtubule pelleting assay is used to show the amount of tubulin incorporated into microtubules under conditions that favor polymerization. Polymerized tubulin is contained in the pellet (P) and unpolymerized tubulin is contained in the supernatant (S) and is quantified using Western blot staining and imaged with Licor software. The red channel depicts alpha tubulin proteins. The green channel demonstrates TUBB4A-GFP. Results are normalized to WT TUBB4A-GFP. (**B**) Quantification of the fractionation of tubulin in the microtubule pellet vs. total tubulin (supernatant and pellet) shows TUBB4A-GFP containing mutations R2G, D249N, and N414K did not alter the fraction of WT tubulin in microtubules (red channel). However, TUBB4A-GFP with mutations in V255I and R282P, which cause primarily hypomyelinating phenotypes, resulted in statistically significant decrease in the fraction of tubulin in the microtubule pellet. (Error bars represent standard error of the mean, $n = 3$, *$P < 0.05$, calculated by one way ANOVA). (**C**) Quantification of the fraction of TUBB4A-GFP polymerized in microtubules shows no alterations resulting from mutations as compared with wild type TUBB4A. All of TUBB4A-GFP, for all six conditions, is incorporated into the tubulin polymer. (**D**) Live imaging of EB3-cherry is visualized by viewing successive frames as different channels, red, green, and blue, creating a 'rainbow' effect. More rapid polymerizations result in a longer rainbow with less overlap between the colors and slower polymerizations results in a shorter rainbow with greater overlap in colors manifested as white. Thus, when there is less overlap in channels as seen in the transfection with wild type TUBB4A-GFP (left) polymerization is faster and when comets are shorter and appear white microtubule elongation is slower as in the case of the V255I (right). Scale bar - 20 μm. (**E**) High power view of EB3 'rainbow' comets show that TUBB4A mutations associated with an isolated hypomyelination phenotype (V255I and R282P) cause a decrease in the length of the EB3 'rainbow' with greater amounts of overlap (white), indicating a slower rate of polymerization. Again, a scale bar 5 μm is shown. (**F**) Quantification of the EB3 comet velocity demonstrates increased velocity of the EB3-cherry comet in D249N (1.85 μm/s), and N414K (1.87 μm/s) when compared with WT TUBB4A-GFP (1.67 μm/s) velocities. Mutations V255I (1.47 μm/s) and R282P (1.31 μm/s), which cause primarily hypomyelinating phenotypes, both had slower EB3 comet velocities indicating a slower rate of microtubule elongation when compared with wild type TUBB4A. (Error bars represent standard error of the mean, $n = 2$ at least 80 comets were counted per condition, **$P < 0.01$, ***$P < 0.001$, calculated by one-way ANOVA).

amount of tubulin that is polymerized, shown above (Fig. 4A and B).

Selective TUBB4A mutations result in altered morphology of cerebellar granule neurons

To further determine pathogenic specificity of *TUBB4A* mutations, we examined their effects in relevant cell types. Because cerebellar granule neurons degenerate in individuals with H-ABC, we tested the effects of our panel of *TUBB4A* mutations on these cells. Cerebellar granule neurons transfected with mutations causing DYT4 or H-ABC phenotypes, p.Arg2Gly, p.Asp249Asn respectively, had morphologically abnormal neurons when compared with WT-transfected neurons (Fig. 5A–C). Neurons transfected with TUBB4A-GFP bearing these mutations had shorter axons, lower number of dendrites, and less branching of the dendritic arbors (Fig. 5G). In contrast, primary cerebellar granule neurons transfected with TUBB4A-GFP plasmids with p.Val255Ile and p.Arg282Pro mutations, which are causative for later onset primary hypomyelination, and the severe infantile form without basal ganglia involvement, p.Asn414Lys,
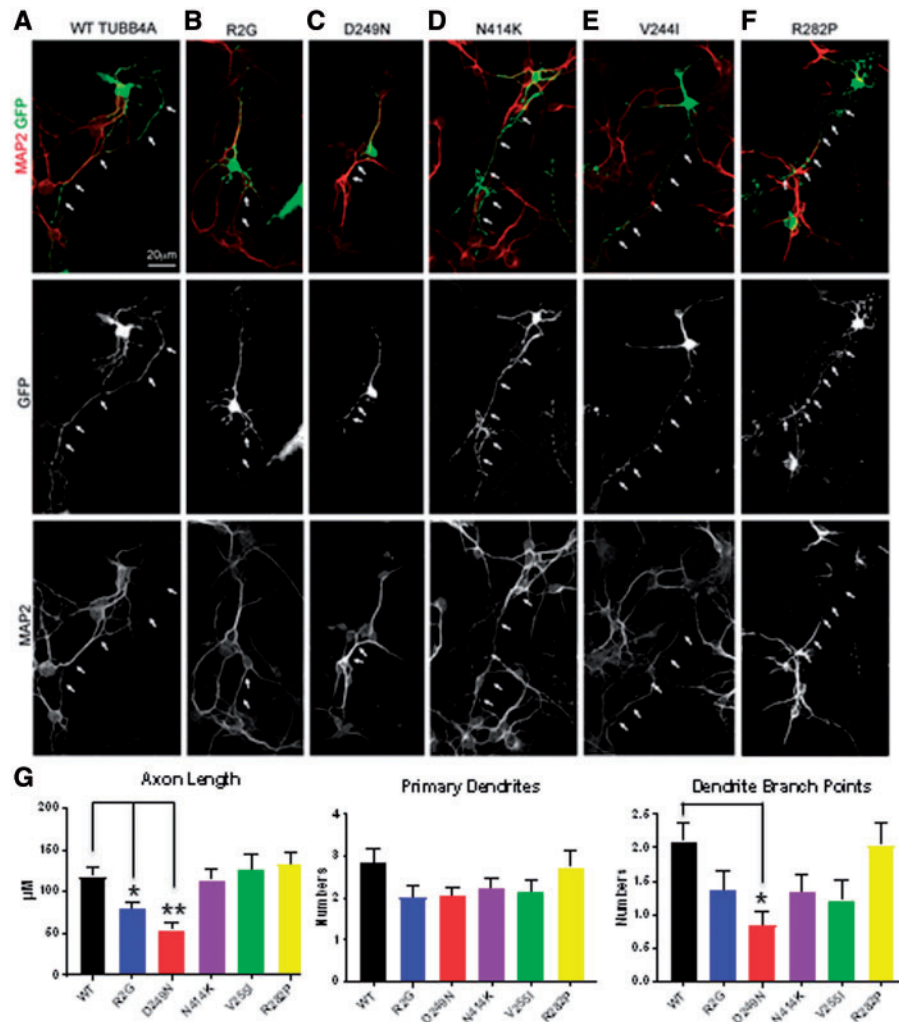
Figure 5. Neuronal morphology is altered in TUBB4A mutations causing neuronal phenotypes. Cerebellar granule neurons were cultured and transfected wild type and mutant TUBB4A-GFP. Neuronal morphology was visualized by GFP (green channel), and MAP2 immunostaining (red channel) is used to differentiate dendrites vs. axons (white arrows). A scale bar (10 μm) is shown. (**G**) Quantification of morphology of cerebellar granule neurons is shown including axon length, and dendrite numbers and branch point. Error bars represent standard error of the mean, $n = 4$, at least 15 transfected neurons were counted for a total of >60 neurons per condition, $^*P < 0.05$, $^{**}P < 0.01$, calculated by one way ANOVA).

had normal neuronal morphology (Fig. 5D–F). They displayed normal axon lengths, dendrite number, and branching of the dendritic arbors when compared with cerebellar granule neurons transfected with WT Tubb4a (Fig. 5G).

Tubulin mutations show differential effects on myelin gene expression and morphology in Oli-neu cells

Oli-neu cells are immortalized cell lines derived from primary mouse oligodendrocytes and have been extensively used to study oligodendrocyte regulation and function (32). These cells can be induced to differentiate into cell types that exhibit branching and expression of the major myelin genes similar to mature oligodendrocytes. We transfected the various tubulin constructs into Oli-neu cells to determine the effect of the different tubulin mutations on oligodendrocyte function. We observed that the p.Arg2Gly mutation had no impact on the expression of the major myelin genes *plp1, mbp* or *cnp* when compared with the WT tubulin construct (Fig. 6A). However, the p.Asp249Asn, p.Arg282Pro and p.Asn414Lys mutations showed

a significant reduction in the expression of all three of the myelin genes while p.Val255Ile showed a significant reduction only in *cnp* gene expression (Fig. 6A).

Oligodendrocyte branching is critical for normal myelination and a functional microtubule network is essential for this process (33,34). We therefore sought to determine whether tubulin mutations could compromise oligodendrocyte branching. Consistent with our myelin gene expression results, we observed that cells transfected with the p.Arg2Gly mutation did not show any differences with respect to Oli-neu branching when compared with the wild type. However, Oli-neu cells transfected with p.Asp249Asn, p.Arg282Pro, p.Val255Ile and p.Asn414Lys mutations showed a significant reduction in the proportion of cells that showed complex branching patterns (Fig. 6B and C).

Discussion

Recently, there has been growing research into a group of disorders collectively known as 'Tubulinopathies' or mutations in
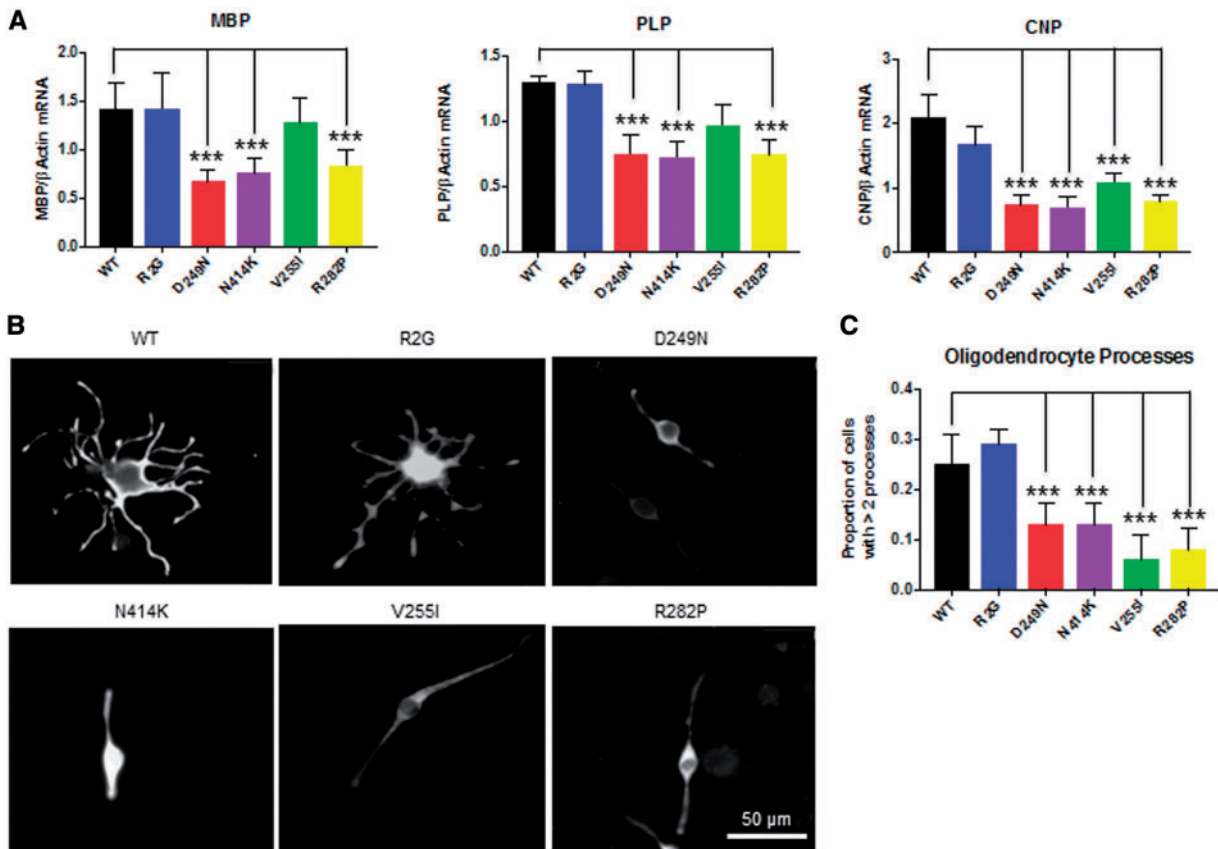
Figure 6. Tubulin mutations impact myelin gene expression and branching in differentiated Oli-neu cells. (**A**) Relative expression levels of mRNA for the myelin genes *Mbp, Plp* and *Cnp* obtained by qRT-PCR from differentiated Oli-neu cells transfected with the different tubulin plasmids. Values were normalized to *β Actin* taking mean value for the mock transfection as 1. Error bars represent standard error of the mean, $n \geq 3$ independent experiments for each construct, ***$P < 0.001$, calculated by one-way ANOVA with Dunnet's post hoc test. (**B**) Representative images of the Oli-neu cells transfected with the different GFP tagged-tubulin mutations. Immuno-staining using the GFP antibody is shown. Scale - 50 μM. (**C**) Proportion of the cells with more than two processes. Error bars are 95% confidence intervals. $n = 3$, more than 150 cells were counted for each replicate, ***$P < 0.001$, calculated by Z-test.

tubulin isoforms that cause a spectrum of disorders. Thus far mutations in *TUBA1A, TUBA4A, TUBB2A, TUBB2B, TUBB3, TUBB4A, TUBB5*, and *TUBG1* have been identified as causing a neurologic disease phenotype (24). Here, we present evidence demonstrating that mutations in *TUBB4A* cause distinct phenotypes in neurons, oligodendrocytes, and both cell types.

Our data suggest that the broad spectrum of clinical phenotypes due to *TUBB4A* mutations [Whispering dysphonia (DYT4)], isolated hypomyelination with cerebellar atrophy, early infantile encephalopathy and H-ABC) may be due to the selective cellular impact and microtubule dynamics of different mutations. Indeed, each mutation appears different in its effects on microtubule dynamics and cellular morphology (Table 2).

The DYT4 clinical phenotype is the most distinctive, with its adult onset phenotype and isolated dystonia without any white matter abnormalities on neuroimaging. Consistent with this finding, the p.Arg2Gly mutation responsible for DYT4 had alterations in neuronal morphology and was the only one of the mutations without any alterations in oligodendrocyte morphology or myelin gene expression. This phenotype thus appears to be the result of selective neuronal involvement.

Conversely, the mutations associated with isolated hypomyelination (p.Val255Ile and p.Arg282Pro) and infantile encephalopathy (p.Asn414Lys) all significantly down-regulated myelin gene expression and branching complexity when expressed in Oli-neu cells but had no impact on neuronal morphology in

transfected cells. Overall, these mutations (p.Val255Ile, p.Arg282Pro, and p.Asn414Lys) appear to have a predominant oligodendrocyte involvement. In keeping with the significant hypomyelination seen in individuals, it could be hypothesized that the atrophy of the cerebellum seen in some cases might be a consequence of glial abnormalities rather than an independent neuronal abnormality.

The canonical H-ABC mutation (p.Asp249Asn) was the only mutation tested in this subset that altered both neuronal and oligodendrocyte morphology *in vitro* and the expression of myelin genes. These findings were consistent with a clinical phenotype and neuropathological phenotype that affected both neurons and oligodendrocytes.

On neuropathology, the individuals with canonical H-ABC have severe involvement of the cerebellar cortex affecting both the neurons in the granular layer and the Purkinje cells and marked loss of putaminal neurons with axonal swelling. These individuals also have marked loss of oligodendrocytes, thus mimicking the combined neuronal and oligodendrocyte involvement seen *in vitro*. It should be noted that neuropathology further reflects the specificity of different mutations as in the p.Asn414Lys mutation the neostriatum is intact despite severe hypomyelination and oligodendrocyte density is highly increased. This divergent effect on oligodendrocyte numbers could be due to differences in neuroaxonal involvement between H-ABC and the infantile onset encephalopathy

Table 2. Pathologic and in vitro functional effects of specific mutations

Disease description	Whispering dysphonia (DYT4)	H-ABC	Isolated hypomyelination	Isolated hypomyelination	Early infantile encephalopathy
Amino acid change	R2G	D249N	V255I	R282P	N414K
Presence of abnormal morphology of transfected cells *in vitro*	Neuronal only	Neuronal and oligodendrocyte	Oligodendrocyte only	Oligodendrocyte only	Oligodendrocyte only
Microtubule dynamics	Normal	Abnormal, increased polymerization	Abnormal, decreased polymerization	Abnormal, decreased polymerization	Abnormal, increased polymerization
Myelin protein expression	Normal	Decreased	Decreased	Decreased	Decreased
Human pathology	Not available	Available	Not available	Not available	Available
Striatal neurons		Loss with axonal spheroids			Spared
Oligodendrocytes		Loss with decreased number of oligodendrocytes			Increased density of oligodendrocytes
Myelination		Hypomyelination			Hypomyelination
Cerebellar granular layer/Purkinje cells		Affected			Affected

associated with p.Asn414Lys. Early-onset neuronal and axonal diseases are typically associated with oligodendrocyte loss in the white matter (35–37). By contrast, oligodendrocyte progenitor proliferation is a common reaction to lack of myelin when axons are relatively spared (38).

All the mutations with a hypomyelination phenotype altered microtubule dynamics. In contrast to decreased polymerization caused by mutations with isolated hypomyelination (p.Val255Ile and p.Arg282Pro), increased polymerization was detected by EB3 comet analysis for p.Asp249Asn and p.Asn414Lys and while this effect was small, it was statistically significant. This suggests that imbalances in tubulin dynamics, in either direction, can cause a disease phenotype. p.Val255Ile and p.Arg282Pro altered the ability of WT tubulin to incorporate into microtubules suggesting these mutations cause a dominant toxic gain of function. The other two mutations affecting tubulin polymerization, p.Asp249Asn and p.Asn414Lys, increased the rate of polymerization. It should be noted that p.Asn414Lys has recently been shown in humans to demonstrate the accumulation of microtubules in oligodendrocytes (25). Conversely, p.Arg2Gly did not affect microtubule dynamics to a detectable level, suggesting that this mutation might act through a distinct mechanism. However, it is also possible, given the milder phenotype of this mutation that defects were too mild to be detected by our assays. It should be noted that the p.Arg2Gly mutation is located in a highly conserved MREI region and is thought to interact with p.Asp249Asn at a salt bridge to modulate protein stability (10). The p.Arg2Gly mutation may cause defects in tubulin function through mechanisms that are unrelated to its dynamic state, including trafficking and transport that we have not explored in the present study (39).

Although the exact role of TUBB4A in myelination is still unclear, microtubules play a critical role in the formation of normal myelin. Of note, the transport of key myelin mRNA and proteins to the myelin sheet is microtubule-dependent. The PLP protein is synthesized in membrane-bound ribosomes and transported through the Golgi to myelin by a vesicular, microtubule-dependent process (40,41). *Mbp* mRNA is transported on microtubules to the myelin compartment and this translocation is perturbed in cultured oligodendrocytes by drugs affecting microtubule dynamics (42). Additionally, CNP participates in the structural support system needed to maintain cell processes of oligodendrocytes by copolymerizing with tubulin and inducing microtubule assembly (43). In the case of the *taiep* mutant, a rat model in which a p.Ala302Thr homozygous mutation in the rat *tubb4a* gene was recently identified, progressive demyelination is thought to be due to an abnormal accumulation of microtubules in oligodendrocytes (25). Interestingly, oligodendrogliosis and accumulation of microtubules in oligodendrocytes are also found on human autopsy specimens with the heterozygous variant p.Asn414Lys, which leads to severe hypomyelenation and infantile encephalopathy (25). Our EB3 comet assay demonstrated an increased rate of polymerization suggesting that an alteration in tubulin polymerization may affect microtubule accumulation in both the taeip rat and in the infantile encephalopathy caused by the p.Asn414Lys mutation. The 3D modeling of the Tubb4a protein suggests the p.Asn414Lys mutation alters a binding site for kinesin and other motor proteins (Fig. 3); additionally, the taeip rats have also demonstrated reduced levels and altered trafficking of MBP mRNA both *in vivo* and *in vitro* (44,45). Our findings of reduced expression of *mbp*, *plp* and *cnp* might thus be a consequence of altered trafficking of the cognate mRNA molecules for these genes, either as a result of abnormal binding of motor proteins or an abnormal accumulation of microtubules and disruption of cell trafficking. Pharmacological disruption of microtubules has also been shown to compromise oligodendrocyte outgrowth and branching (46), a phenomenon that we have observed with all the four *TUBB4A* mutations that cause the hypomyelination phenotype.

The developmental and cellular regulation of TUBB4A expression have not been studied in detail. However, global gene expression analysis in different CNS cell types suggests that this gene has a higher expression in mature oligodendrocytes when compared with neurons, astrocytes or oligodendrocyte precursor cells. Combined with our data indicating cell-specific effects, this would suggest a mechanism that favors a cell autonomous role for the TUBB4A mutations in oligodendroglial

function. However, it must be kept in mind that these are *in vitro* studies and that in an *in vivo* setting with complex cellular interactions that these mutations might have secondary non-cell autonomous consequences. Developmental effects of these mutations have also not been addressed in our experiments. Further studies in whole organisms (25) with *TUBB4A* mutations are necessary to elucidate these mechanisms.

Clinicians typically differentiate between 'neuronal' and non-neuronal disorders based on clinical and radiologic features. In some disorders considered to be primarily neuronal, white matter abnormalities on neuroimaging are visible and are hypothesized to be due to secondary glial dysfunction attributed to abnormal neuronal signaling (2). Conversely, H-ABC is part of a group of disorders called leukodystrophies, defined as affecting the glial-axonal unit. In these disorders, symptoms attributable to neuronal dysfunction are classically ascribed to secondary injury to unmyelinated axons. However, in DYT4, H-ABC and other *TUBB4A* mutations, specific mutations in a single gene appear to be the result of cell selective phenotypes with mutations that lead to either purely neuronal, combined neuronal and oligodendrocytic, or purely oligodendrocytic defects closely matching their respective clinical phenotypes. This suggests that underlying cellular physiology in these disorders may be more complex than initially hypothesized, with mutations in the same gene having distinct but important impacts in different and sometimes several cell types. Cell specificity of different mutations in *TUBB4A* related disorders may be indicative of a broader phenomenon also likely to be present in other neurogenetic disorders currently characterized on a clinical or radiologic basis as primarily neuronal or leukodystrophies. As cell targeted molecular therapies are developed, these considerations will have a growing importance in disease management.

Supplementary Material

Supplementary Material is available at *HMG* online.

Acknowledgements

Funding

References

1. Hamilton, E.M., Polder, E., Vanderver, A., Naidu, S., Schiffmann, R., Fisher, K., Raguž, A.B., Blumkin, L., van Berkel, C.G.M., Waisfisz, Q. *et al.* (2014) Hypomyelination with atrophy of the basal ganglia and cerebellum: further delineation of the phenotype and genotype-phenotype correlation. *Brain*, **137**, 1921–1930.
2. Schiffmann, R. and van der Knaap, M.S. (2009) Invited article: an MRI-based approach to the diagnosis of white matter disorders. *Neurology*, **72**, 750–759.
3. Lohmann, K., Wilcox, R.A., Winkler, S., Ramirez, A., Rakovic, A., Park, J.S., Arns, B., Lohnau, T., Groen, J., Kasten, M. *et al.* (2013) Whispering dysphonia (DYT4 dystonia) is caused by a mutation in the TUBB4 gene. *Ann. Neurol.*, **73**, 537–545.
4. Hersheson, J., Mencacci, N.E., Davis, M., MacDonald, N., Trabzuni, D., Ryten, M., Pittman, A., Paudel, R., Kara, E., Fawcett, K. *et al.* (2013) Mutations in the autoregulatory domain of beta-tubulin 4a cause hereditary dystonia. *Ann. Neurol.*, **73**, 546–553.
5. Kumar, K.R., Vulinovic, F., Lohmann, K., Park, J.S., Schaake, S., Sue, C.M. and Klein, C. (2015) Mutations in TUBB4A and spastic paraplegia. *Mov. Disord.*, **30**, 1857–1858.
6. Sagnelli, A., Magri, S., Farina, L., Chiapparini, L., Marotta, G., Tonduti, D., Consonni, M., Scigliuolo, G.M., Benti, R., Pareyson, D. *et al.* (2016) Early-onset progressive spastic paraplegia caused by a novel TUBB4A mutation: brain MRI and FDG-PET findings. *J. Neurol.*, **263**, 591–593.
7. Kancheva, D., Chamova, T., Guergueltcheva, V., Mitev, V., Azmanov, D.N., Kalaydjieva, L., Tournev, I. and Jordanova, A. (2015) Mosaic dominant TUBB4A mutation in an inbred family with complicated hereditary spastic paraplegia. *Mov. Disord.*, **30**, 854–858.
8. Isakov, O., Lev, D., Blumkin, L., Celniker, G., Leshinsky-Silver, E. and Shomron, N. (2015) Crowdfunding effort identifies the causative mutation in a patient with nystagmus, microcephaly, dystonia and hypomyelination. *J. Genet. Genomics*, **42**, 79–81.
9. Pizzino, A., Pierson, T.M., Guo, Y., Helman, G., Fortini, S., Guerrero, K., Saitta, S., Murphy, J.L., Padiath, Q., Xie, Y. *et al.* (2014) TUBB4A de novo mutations cause isolated hypomyelination. *Neurology*, **83**, 898–902.
10. Simons, C., Wolf, N.I., McNeil, N., Caldovic, L., Devaney, J.M., Takanohashi, A., Crawford, J., Ru, K., Grimmond, S.M., Miller, D. *et al.* (2013) A de novo mutation in the beta-tubulin gene TUBB4A results in the leukoencephalopathy hypomyelination with atrophy of the basal ganglia and cerebellum. *Am. J. Hum. Genet.*, **92**, 767–773.
11. van der Knaap, M.S., Naidu, S., Pouwels, P.J., Bonavita, S., van Coster, R., Lagae, L., Sperner, J., Surtees, R., Schiffmann, R. and Valk, J. (2002) New syndrome characterized by hypomyelination with atrophy of the basal ganglia and cerebellum. *Am. J. Neuroradiol.*, **23**, 1466–1474.
12. Blumkin, L., Halevy, A., Ben-Ami-Raichman, D., Dahari, D., Haviv, A., Sarit, C., Lev, D., van der Knaap, M.S., Lerman-Sagie, T. and Leshinsky-Silver, E. (2014) Expansion of the spectrum of TUBB4A-related disorders: a new phenotype associated with a novel mutation in the TUBB4A gene. *Neurogenetics*, **15**, 107–113.
13. Ferreira, C., Poretti, A., Cohen, J., Hamosh, A. and Naidu, S. (2014) Novel TUBB4A mutations and expansion of the neuroimaging phenotype of hypomyelination with atrophy of the basal ganglia and cerebellum (H-ABC). *Am. J. Med. Genet. A*, **164**, 1802–1807.
14. Miyatake, S., Osaka, H., Shiina, M., Sasaki, M., Takanashi, J., Haginoya, K., Wada, T., Morimoto, M., Ando, N., Ikuta, Y. *et al.* (2014) Expanding the phenotypic spectrum of TUBB4A-associated hypomyelinating leukoencephalopathies. *Neurology*, **82**, 2230–2237.
15. Vemula, S.R., Xiao, J., Bastian, R.W., Momcilovic, D., Blitzer, A. and LeDoux, M.S. (2014) Pathogenic variants in TUBB4A are not found in primary dystonia. *Neurology*, **82**, 1227–1230.
16. Carvalho, D., Santos, S., Martins, B. and Marques, F.P. (2015) TUBB4A novel mutation reinforces the genotype-phenotype correlation of hypomyelination with atrophy of the basal ganglia and cerebellum. *Brain*, **138**, e327.
17. Erro, R., Hersheson, J., Houlden, H. and Bhatia, K.P. (2015) A novel TUBB4A mutation suggests that genotype-phenotype

correlation of H-ABC syndrome needs to be revisited. *Brain*, **138**, e370.

18. Nicita, F., Bertini, E., Travaglini, L., Armando, M. and Aiello, C. (2016) Congenital-onset spastic paraplegia in a patient with TUBB4A mutation and mild hypomyelination. *J. Neurol. Sci.*, **368**, 145–146.

19. Tonduti, D., Aiello, C., Renaldo, F., Dorboz, I., Saaman, S., Rodriguez, D., Fettah, H., Elmaleh, M., Biancheri, R., Barresi, S. *et al.* (2016) TUBB4A-related hypomyelinating leukodystrophy: New insights from a series of 12 patients. *Eur. J. Paediatr. Neurol.*, **20**, 323–330.

20. Arai-Ichinoi, N., Uematsu, M., Sato, R., Suzuki, T., Kudo, H., Kikuchi, A., Hino-Fukuyo, N., Matsumoto, M., Igarashi, K., Haginoya, K. *et al.* (2016) Genetic heterogeneity in 26 infants with a hypomyelinating leukodystrophy. *Hum. Genet.*, **135**, 89–98.

21. Erro, R., Hersheson, J., Ganos, C., Mencacci, N.E., Stamelou, M., Batla, A., Thust, S.C., Bras, J.M., Guerreiro, R.J., Hardy, J. *et al.* (2015) H-ABC syndrome and DYT4: Variable expressivity or pleiotropy of TUBB4 mutations?. *Mov. Disord.*, **30**, 828–833.

22. Purnell, S.M., Bleyl, S.B. and Bonkowsky, J.L. (2014) Clinical exome sequencing identifies a novel TUBB4A mutation in a child with static hypomyelinating leukodystrophy. *Pediatr. Neurol.*, **50**, 608–611.

23. Shimojima, K., Okumura, A., Ikeno, M., Nishimura, A., Saito, A., Saitsu, H., Matsumoto, N. and Yamamoto, T. (2015) A de novo TUBB4A mutation in a patient with hypomyelination mimicking Pelizaeus-Merzbacher disease. *Brain Dev.*, **37**, 281–285.

24. Chakraborti, S., Natarajan, K., Curiel, J., Janke, C. and Liu, J. (2016) The emerging role of the tubulin code: From the tubulin molecule to neuronal function and disease. *Cytoskeleton (Hoboken)*, **73**, 521–550.

25. Duncan, I.D., Bugiani, M., Radcliff, A.B., Moran, J.J., Lopez-Anido, C., Duong, P., August, B.K., Wolf, N.I., Knaap, M.S.V. and Svaren, J. (2017) A mutation in the Tubb4a gene leads to microtubule accumulation with hypomyelination and demyelination. *Ann. Neurol.*, **81**, 690–702.

26. Liu, J.S., Schubert, C.R., Fu, X., Fourniol, F.J., Jaiswal, J.K., Houdusse, A., Stultz, C.M., Moores, C.A. and Walsh, C.A. (2012) Molecular basis for specific regulation of neuronal kinesin-3 motors by doublecortin family proteins. *Mol. Cell*, **47**, 707–721.

27. Lee, H.Y., Greene, L.A., Mason, C.A. and Manzini, M.C. (2009) Isolation and culture of post-natal mouse cerebellar granule neuron progenitor cells and neurons. *J. Vis. Exp.*, **16**, pii: 990.

28. Livak, K.J. and Schmittgen, T.D. (2001) Analysis of relative gene expression data using real-time quantitative PCR and the 2(-Delta Delta C(T)) Method. *Methods*, **25**, 402–408.

29. Lowe, J., Li, H., Downing, K.H. and Nogales, E. (2001) Refined structure of alpha beta-tubulin at 3.5 A resolution. *J. Mol. Biol.*, **313**, 1045–1057.

30. Gigant, B., Wang, W., Dreier, B., Jiang, Q., Pecqueur, L., Pluckthun, A., Wang, C. and Knossow, M. (2013) Structure of a kinesin-tubulin complex and implications for kinesin motility. *Nat. Struct. Mol. Biol.*, **20**, 1001–1007.

31. Ti, S.C., Pamula, M.C., Howes, S.C., Duellberg, C., Cade, N.I., Kleiner, R.E., Forth, S., Surrey, T., Nogales, E. and Kapoor, T.M. (2016) Mutations in Human Tubulin Proximal to the Kinesin-Binding Site Alter Dynamic Instability at Microtubule Plus- and Minus-Ends. *Dev. Cell*, **37**, 72–84.

32. De Vries, G.H. and Boullerne, A.I. (2010) Glial cell lines: an overview. *Neurochem. Res.*, **35**, 1978–2000.

33. Baumann, N. and Pham-Dinh, D. (2001) Biology of oligodendrocyte and myelin in the mammalian central nervous system. *Physiol. Rev.*, **81**, 871–927.

34. Richter-Landsberg, C. (2008) The cytoskeleton in oligodendrocytes. Microtubule dynamics in health and disease. *J. Mol. Neurosci.*, **35**, 55–63.

35. Bugiani, O. and Borrone, C. (1976) Fucosidosis: a neuropathological study. *Riv. Patol. Nerv. Ment.*, **97**, 133–141.

36. Haberland, C., Brunngraber, E., Witting, L. and Brown, B. (1973) The white matter in G M2 gangliosidosis. A comparative histopathological and biochemical study. *Acta Neuropathol.*, **24**, 43–55.

37. van der Voorn, J.P., Kamphorst, W., van der Knaap, M.S. and Powers, J.M. (2004) The leukoencephalopathy of infantile GM1 gangliosidosis: oligodendrocytic loss and axonal dysfunction. *Acta Neuropathol.*, **107**, 539–545.

38. Bugiani, M., Boor, I., van Kollenburg, B., Postma, N., Polder, E., van Berkel, C., van Kesteren, R.E., Windrem, M.S., Hol, E.M., Scheper, G.C. *et al.* (2011) Defective glial maturation in vanishing white matter disease. *J. Neuropathol. Exp. Neurol.*, **70**, 69–82.

39. Fu, M.M. and Holzbaur, E.L. (2014) Integrated regulation of motor-driven organelle transport by scaffolding proteins. *Trends Cell Biol.*, **24**, 564–574.

40. Bizzozero, O.A., Pasquini, J.M. and Soto, E.F. (1982) Differential effect of colchicine upon the entry of proteins into myelin and myelin related membranes. *Neurochem. Res.*, **7**, 1415–1425.

41. Townsend, L.E. and Benjamins, J.A. (1983) Effects of monensin on posttranslational processing of myelin proteins. *J. Neurochem.*, **40**, 1333–1339.

42. Carson, J.H., Worboys, K., Ainger, K. and Barbarese, E. (1997) Translocation of myelin basic protein mRNA in oligodendrocytes requires microtubules and kinesin. *Cell Motil. Cytoskeleton*, **38**, 318–328.

43. Lee, J., Gravel, M., Zhang, R., Thibault, P. and Braun, P.E. (2005) Process outgrowth in oligodendrocytes is mediated by CNP, a novel microtubule assembly myelin protein. *J. Cell Biol.*, **170**, 661–673.

44. O'Connor, L.T., Goetz, B.D., Couve, E., Song, J. and Duncan, I.D. (2000) Intracellular distribution of myelin protein gene products is altered in oligodendrocytes of the taiep rat. *Mol. Cell Neurosci.*, **16**, 396–407.

45. Song, J., Carson, J.H., Barbarese, E., Li, F.Y. and Duncan, I.D. (2003) RNA transport in oligodendrocytes from the taiep mutant rat. *Mol. Cell Neurosci.*, **24**, 926–938.

46. Song, J., Goetz, B.D., Baas, P.W. and Duncan, I.D. (2001) Cytoskeletal reorganization during the formation of oligodendrocyte processes and branches. *Mol. Cell Neurosci.*, **17**, 624–636.

47. Biasini, M., Bienert, S., Waterhouse, A., Arnold, K., Studer, G., Schmidt, T., Kiefer, F., Cassarino, T.G., Bertoni, M., Bordoli, L. *et al.* (2014) SWISS-MODEL: modelling protein tertiary and quaternary structure using evolutionary information. *Nucleic Acids Res.*, **42**, W252–W258.